Agricultural and Forest Meteorology 359 (2024) 110278

Contents lists available at ScienceDirect

Agricultural and Forest Meteorology

journal homepage: www.elsevier.com/locate/agrformet

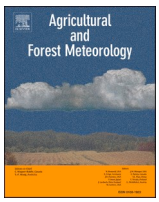

Partitioning and driver analysis of eddy covariance derived N_2O emissions from a grazed and fertilized pasture

Lena Barczyk [a,b,*], Johan Six [b], Christof Ammann [a]

[a] Climate and Agriculture group, Agroscope Research Station, Reckenholzstrasse 191, 8046, Zürich, Switzerland
[b] Department of Environmental Systems Science, ETH Zürich, Universitätstrasse 2, 8092, Zürich, Switzerland

ARTICLE INFO

Keywords:
Pasture
Nitrous oxide
Eddy covariance
Random forest
Flux partitioning
Emission driver

ABSTRACT

Managed pastures are strong sources for the greenhouse gas nitrous oxide (N_2O) through various nitrogen (N) inputs. So far, chamber measurements have been used to quantify N_2O emissions and emissions factors of specific emissions sources like grazing cattle excreta. This study presents a three-year dataset of N_2O emissions from a grazed and fertilized pasture measured by eddy covariance (EC) in eastern Switzerland. N_2O fluxes were gap-filled and disaggregated into the emission sources (flux partitioning) by using random forest. The excreta N deposition in the pasture was estimated based on a cattle nitrogen budget approach using observed milk yield, body weight and feed intake of the cattle herd. Furthermore, a driver analysis was performed to quantify the relationship between N_2O emissions and predictor variables. The observed annual N_2O emissions amounted to 5.3 ± 0.8, 3.1 ± 0.5 and 4.4 ± 0.7 kg N_2O-N ha^{-1} yr^{-1} and were disaggregated into background, fertilizer and excreta related N_2O emissions with contributions of 27–46 %, 15–40 % and 30–51 %, respectively. Combining the excreta N_2O fluxes with the excreta N inputs resulted in an average emission factor (EF) for cattle excreta of 1.1 ± 0.5 %, that tends to be higher than the IPCC default value of 0.6 % for wet climates. While maximum N_2O emissions usually were observed after fertilizer application and under optimum soil moisture conditions as expected, distinct N_2O emission peaks also occurred during a longer drought period in summer and could be parametrised as a function of precipitation and previous grazing activity. Moreover, peak N_2O emissions occurred during the cold season at low temperatures and should be considered in future studies. Overall, we suggest that EC measurements under pasture conditions with subsequent flux partitioning by random forest are suitable for quantifying pasture N_2O emissions of different sources.

1. Introduction

Nitrous oxide (N_2O) is a powerful greenhouse gas (GHG) with a global warming potential ~300 times higher than carbon dioxide (CO_2) and is an ozone depleting molecule. Agricultural systems emit substantial amounts of N_2O, accounting for more than 50 % of global anthropogenic N_2O emissions (Kroeze et al. 1999; IPCC 2006). Nitrogen (N) input from N-fertilizers and excreta of grazing cattle is the main culprit for these emissions (Russelle 1992; Zheng et al. 2023). However, N inputs via harvest residues, atmospheric deposition (Ackermann et al. 2019; Du et al. 2021) and biological fixation (Reinsch et al. 2020) need to be taken into account too.

Pasture systems are particularly vulnerable to N_2O emissions, through excreta of grazing cattle containing essential amounts of N up to 2000 kg N ha^{-1} (Selbie et al. 2015). For the calculation and reporting of N_2O emissions ($F(N_2O)$) from pasture systems at the national scale following the IPCC guidelines, annual average emission factors (EF) are used, i.e., the fraction of N inputs (I_N) emitted as N_2O. In the default IPCC methodology of Tier 1, a common emission factor (EF_1) of 1 % is used for fertilization (fertil), atmospheric N deposition (dep) and harvest residues (resid). The default value (EF_3) for cattle excreta is 0.4 %, disaggregated into 0.6 % for wet climates and 0.2 % for dry climates (IPCC 2006; IPCC 2019). Hence, the total $F(N_2O)$ is calculated as:

$$F(N_2O) = EF_1 \cdot \left(I_{N-fertil} + I_{N-dep} + I_{N-resid}\right) + EF_3 \cdot I_{N-excreta} \quad (1)$$

However, the global default EF_3 value is based on limited experimental studies, mainly from New Zealand and the United Kingdom (Beltran et al. 2021), and may not reflect regional conditions. The data availability for EF_1 is greater though. However, reported observed values for both EF_3 and EF_1 show large variabilities (Luo et al. 2019;

* Corresponding author.
E-mail address: lena.barczyk@agroscope.admin.ch (L. Barczyk).

https://doi.org/10.1016/j.agrformet.2024.110278
Received 23 April 2024; Received in revised form 8 October 2024; Accepted 19 October 2024

Walling et al. 2020). This is also why it is recommended to adopt higher Tiers, e.g. country-specific EFs, to improve the quantification of N_2O emissions at the national scale. Emissions resulting from $I_{N\text{-}resid}$ and $I_{N\text{-}dep}$ are, like the respective inputs, assumed to occur continuously over the entire growing season or year. Therefore, they are often considered as 'background' fluxes $F(N_2O)_{bg}$, on which fertilizer and excreta related emissions are superimposed.

Chamber measurements have been used in most cases to measure N_2O emissions as they are ideal to observe individual emission sources (like urine/dung patches or fertilizer applications) on small spatial areas (typically $< 1m^2$) together with respective background or control measurements. Therefore, chamber measurements enable the calculation of EF values and the comparison of different treatments (Barczyk et al., 2023; Singh et al., 2021; van Groeningen et al., 2005a,b). However, chambers may alter the microclimate and soil conditions, when inserting frames into the soil, which can affect N_2O production and consumption processes (Duchicela et al. 2021). The spatial heterogeneity of soils (Shi et al. 2021) require many chamber replicates for a precise evaluation of N_2O fluxes which is not feasible in many studies (e.g. for cost reasons or due to time constraints). Furthermore, it is advised to measure with high time resolution (e.g. every two hours) to capture the temporal variability of N_2O fluxes, in particular after N applications and precipitation (van der Weerden et al. 2013; Grace et al. 2020). Automated chamber systems can measure at higher frequencies than manual chambers (Savage et al. 2014; Wang et al. 2016). However, manual chambers are used more often than automated chambers because they require less technical expertise to operate and are less expensive (O'Connell et al. 2022).

Micrometeorological methods like the eddy covariance (EC) method offer several advantages over the chamber method. They measure on scales from several hundred m^2 to several hectares and in a high temporal resolution (commonly at half-hourly time intervals). Thus, they are able to integrate over the spatial heterogeneity of soils, and to encompass multiple emission sources. However, the EC holds limitations like the requirement for homogenous turbulent atmospheric conditions and flat terrain (Nemitz et al. 2018), or the susceptibility to high frequency damping errors (Moncrieff et al. 1996). Furthermore, EC measurements yield a total flux, thus a partitioning is necessary to quantify the contribution of individual N sources. Currently, a combined approach of EC measurements and chambers is considered as the best solution to identify N_2O flux sources (and sinks) and to quantify the contribution of different flux sources (Jones et al. 2011; Voglmeier et al. 2019; Wecking et al. 2020; Murphy et al. 2022). In agricultural ecosystems without grazing, significant N inputs only occur a few times per year through fertilizer applications that are separated by longer time intervals (typically > 1 month). Thus the fertilizer effects can be partitioned from background emissions relatively easily by relatively few simultaneous chamber measurements (e.g. Jones et al. 2011). For grazed systems, however, it is not possible to simulate every single grazing day due to time constraints, thus single chamber experiments on artificially applied excreta patches were performed in Wecking et al. (2020) and Murphy et al. (2022). The results were integrated over the whole grazing season, thereby not accounting for seasonal variabilities linked to changes in soil moisture or temperature. Voglmeier et al. (2019) measured mainly during dry conditions on real urine and dung patches within a three-month measurement campaign, though parameterized urine and dung fluxes as a function of environmental drivers.

One important issue of EC N_2O fluxes is, however, the filling of gaps in the flux time series. Fuchs et al. (2018), for instance, evaluated the effect of fertilization by quantifying N_2O emissions of two differently managed parcels with one EC tower based on the wind direction. Consequently, the flux time series was split into two separate flux time series (for each parcel) causing low data coverages of < 50 %. Furthermore, there is yet no standard gap-filling approach for N_2O fluxes measured by EC. Less complex approaches like linear interpolation, running average or multiple linear regression have been widely used for N_2O gap-filling (Levy et al. 2017; Vinzent et al. 2017; Liang et al. 2018; Voglmeier et al. 2019) and can be appropriate for smaller gaps (e.g. < 1 day). Non-linear, non-parametric approaches like general additive models (GAM) or machine learning (ML) algorithms like artificial neural networks (ANNs) or random forest (RF) appear more appropriate to capture the dynamic character of N_2O, especially when the dataset has larger gaps e.g. up to several weeks (Kim et al. 2019; Taki et al. 2019; Cowan et al. 2020; Goodrich et al. 2021). GAM and ML algorithms can handle large datasets easily and assumptions of classical statistical techniques as normality or constant-variance do not need to be considered. Taki et al. (2019) and Bigaignon et al. (2020) compared linear interpolation and ANN as gap-filling techniques for N_2O, showing a better statistical score and a better prediction of flux variability for ANN.

So far, only a few studies applied RF to gap-fill EC N_2O flux time series (none of these for a grazed pasture) showing a high predictive ability of the RF (Goodrich et al. 2021; Maier et al. 2022; Feigenwinter et al. 2023). Furthermore, Kim et al. (2019) compared three ML algorithms (ANN, RF, and support vector machine) for the gap-filling of EC methane (CH_4) fluxes (like N_2O nonlinearly depending on multiple drivers) showing the best performance for RF. In other research fields, such as modelling ground water nitrate concentrations (He et al. 2022), classification in ecology (Cutler et al. 2007) or in modelling global N_2O emissions from agricultural soils (Perlman et al. 2014), RF generally testified a high accuracy. The RF algorithm constructs a multitude of random decision trees (Rokach et al. 2005) by using a subset of the observations through bootstrapping. To get the final prediction, the predictions of all individual trees are averaged. RF is faster and less prone to overfitting than other ML algorithms like ANN and provides insights into the importance of single predictors (Breimann 2001).

In this study, we conducted EC N_2O measurements over three years at a Swiss pasture site. To our knowledge, this the first study that applied RF for the gap-filling and partitioning of EC N_2O fluxes from a grazed and fertilized pasture. In this way, the contribution of different N_2O emission sources and EF_3 values were quantified from EC fluxes without using the chamber methodology. EF_3 values have been rarely determined by experiments in Central Europe, thus forcing the countries to use IPCC default EF_3 values. Hence, we discuss the suitability of RF for EC flux partitioning and for quantifying reliable EF_3 values.

2. Methods

2.1. Site and experiment description

This study was conducted from April 2020 to April 2023 on a dairy farm at the research station Agroscope Tänikon located in North-Eastern Switzerland (47°29′26.7″N, 8°55′12.1″E; 517 m elevation). The climate is temperate with a mean annual temperature of 9.5 °C and mean annual precipitation of 1124 mm (2009–2019) (MeteoSwiss 2022). The experimental site has been a permanent pasture since 2013. More detailed information about the pasture and soil properties can be found in Barczyk et al. (2023).

The pasture of 2.8 ha (Fig. 1) was divided into four parcels (P1-P4) considering the two main wind directions North-East (NE) and South-West (SW). An EC system was located at the border between P1 and P3 for monitoring N_2O fluxes over three years (2020–2023) from April to April in each year originating from P1 and P3. In addition, a weather station recorded meteorological variables including precipitation. Volumetric soil moisture content (VMC) and soil temperature were measured continuously at four locations in 50 mm depth located in the vicinity of the EC tower (horizontal distances between 1.5 m and 10 m) by using GS3 (Decagon Devices Inc.) and ML3 (Delta-T Devices Ltd.) probes. Water-filled pore space (WFPS) was derived based on VWC and total pore volume determined from soil samples taken at the site.

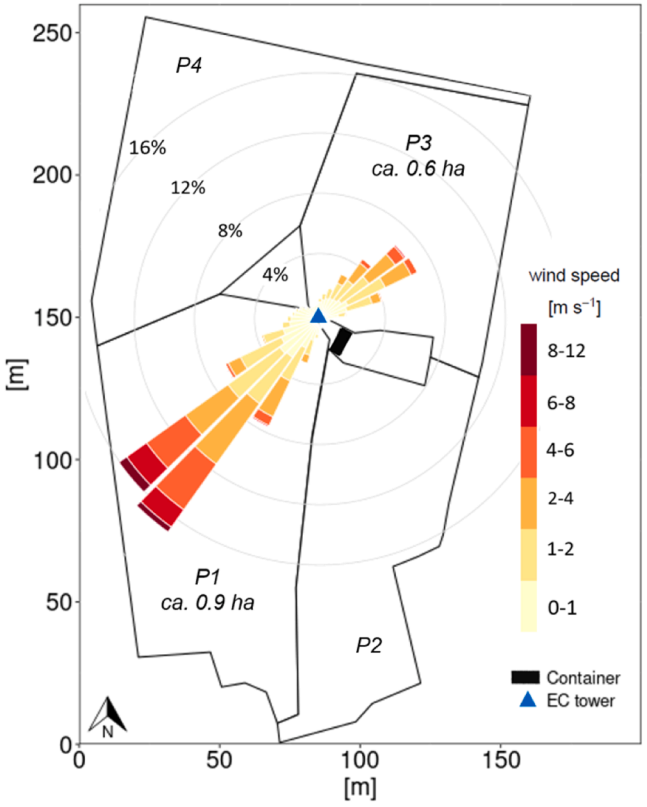

Fig. 1. Map showing the pasture field divided into four parcels with the eddy covariance (EC) tower (blue triangle) and the measurement container (black rectangle) located in the centre. Based on the main wind directions NE and SW, EC fluxes represent parcels P1 and P3.

2.2. Pasture management

During the grazing season (April to the end of October), pasture parcels P1-P4 were grazed alternatingly by two mixed herds of Brown Swiss and Red Holstein dairy cattle. The number of cows per herd ranged from 15 to 20, implying typical stocking densities during grazing of 17–22 cows ha^{-1} for P1 and 25–33 cows ha^{-1} for P3 with parcel sizes of 0.9 ha and 0.6 ha, respectively. The cows only spent part of the day on the pasture, on average about six hours, the remaining time in the barn. However, grazing lengths per day varied considerably (between 1 and 12 h), for instance because of the acclimatization of the cattle to grazing in spring or possible heat stress in the summer months. For the latter reason, cattle grazed during the night at some days in the summer of year 2 and year 3. At some shorter periods of heavy rainfall and/or very wet soil conditions, no grazing took place. In year 1, another research project was performed in the cattle barn for which the cattle stayed in the barn more often and the number of grazing days was lower compared to year 2 and year 3 (Table 2). Hence, the pasture was used for forage production by three harvests and more slurry was applied in year 1 (Table 1). In year 2 and year 3, slurry was applied once in spring and once in autumn. Moreover, synthetic fertilizer applications (Urea, ENTEC26, Ammonium-Nitrate) occurred in year 2 and year 3. In each of the three years, the pasture was mulched at the end of the grazing season (beginning of November), and additionally in late spring to early summer in year 2 and year 3, to remove older vegetation (avoided by the cows) and to stipulate new growth and optimize pasture productivity. Pasture parcels P1 and P3 were managed very similarly, yet grazing was not fully simultaneous but often alternating between the two parcels in year 1 and year 2. Furthermore, P1 received one slurry application more in year 1, and in year 2, the urea application on P3 occurred one week later than on P1. The grazing on P1 and P3 was predominantly alternating in year 1 and year 2, whereas predominantly simultaneous in year 3.

Table 1
Overview of the pasture management including fertilizer applications, harvest and mulching dates for parcels P1 and P3 in the three years (April-April) of the experiment.

	Fertilization date	Fertilizer N applied [kg ha^{-1}]		Fertilizer type	Cutting Date	Cutting type
		P1	P3		P1/P3	
Before	24.02.			Slurry		
Year 1	22.05.	45	31	Slurry	18.05./28.05.	Harvest
	06.07.	31	53	Slurry	30.06.	Harvest
	22.09.	53		Slurry	06.08.	Harvest
	12.11.	65	65	Slurry	10.11.	Mulching
	13.11		57	Slurry		
	24.02.	57		Slurry		
Year 2	22.06.	20		Urea	16.06./02.07.	Mulching
	03.07.		23	Urea	22.10./5.11.	Mulching
	09.11.	69	69	Slurry		
	01.03.	62	62	Slurry		
	07.03.	21	21	ENTEC26		
Year 3	03.06.	30	30	Urea	20.05.	Mulching
	08.11.	53	53	Slurry	08.11.	Mulching
	08.03.	31	31	NH_4NO_3		
	21.03.	35	35	Slurry		

2.3. EC measurements of N_2O fluxes

EC measurements were conducted at a height of 1.8 m and a frequency of 10 Hz from the mid of May 2020 to the end of March 2023. The EC setup consisted of a fast response sonic anemometer (Gill Instruments Ltd., UK) to record wind speed components and sonic temperature and a closed-path quantum cascade laser analyser (QLC, Aerodyne Research Inc., USA) to measure atmospheric N_2O concentrations. N_2O air samples were drawn through a polyamide tube of 3.5 mm inner diameter and 10 m length by a vacuum pump (flow rate around 12 L min^{-1}) to the QCL placed in a temperature-controlled trailer. A customized LabView (National Instruments, US) program was used to combine (synchronize) the data streams of sonic anemometer and QCL in real time, and store them as binary raw data. N_2O fluxes $F(N_2O)$ were calculated as the covariance between the N_2O mixing ratio (x) and the vertical component of the wind speed (w) as

$$F(N_2O) = \rho \cdot \overline{x'w'} \quad (2)$$

over 30 min averaging intervals using EddyPro 7.0.9 (LI-COR Inc., Lincoln, Nebraska, USA). The symbol ρ denotes the average air density. Measurements were initially processed for spikes, amplitude resolution, drop-outs, skewness and kurtosis. The sampling of N_2O through the sampling tube to the QCL caused a time lag between wind components and N_2O air concentrations. In the first step the maximum covariance was searched in a relatively wide lag range (± 20 s). Then the true lag was identified from the distribution of lag values for larger fluxes. It was found that the lags were relatively constant around 1.4 s in the long-term showing minor variations within a range of ± 0.6 s. Therefore, the covariance maximization procedure with default (minimum: 0.8 s; maximum: 2 s; default: 1.4 s) was chosen in EddyPro for compensating the time lag. A linear detrending in the raw (high-frequency) time series was performed to remove possible trend contributions to the flux. For anemometer tilt correction, double wind vector rotation was used. For spectral damping corrections, we used the analytic approach of Moncrieff et al. (2004) in the low-frequency range and the in situ/analytic approach of Fratini et al. (2012) in the high-frequency range. The

quality flag system of Mauder and Foken (2004) was used to rank the quality of calculated fluxes in three classes (qc0: best quality e.g. suitable for driver analysis; qc1: medium quality suitable for annual budget calculations; qc2: bad quality). Furthermore, fluxes were filtered for sufficient turbulent mixing using a friction velocity (u_*) threshold of 0.07 m s^{-1} (Voglmeier et al. 2019), for acceptable tilt angle beta (−2° to 6°) and for the wind direction (SW sector: 170–270° and NE sector: 0–100°) to observe N_2O emissions derived from P1 and P3. Footprint calculations were performed according to Kormann and Meixner (2001) using the calculation procedure described in Neftel et al. (2008). The average footprint contribution of the parcels P1 for south-westerly wind directions and P3 for north-easterly wind directions (see Fig. 1) was 80 % and 84 %, respectively.

2.4. Flux gap filling using random forest

The EC flux quality filtering induced gaps in the $F(N_2O)$ time series. Most of these gaps were relatively short (few hours) and caused by non-stationarity and low turbulence. Besides a six weeks data gap in the beginning of the experiment, the largest gap of four days occurred due to an electrical blackout. Because of the slightly differing pasture management of P1 and P3 (mainly alternating grazing and one additional slurry application on P1), N_2O flux time series were gap filled separately for P1 (SW wind sector) and P3 (NE wind sector). Overall, SW wind directions were slightly more frequent than NE wind directions with 60 % and 40 %, respectively.

Random forest (RF), a non-parametric machine-learning algorithm, was used to gap-fill the flux data time series. Soil water-filled pore space WFPS [%] in 50 mm depth, soil temperature T_s [°C] in 50 mm depth and precipitation P [mm] cumulated over the last 2, 6, 24, 48, 72, 96, 120 h were tested as environmental predictor variables. To account for the N excreted by the grazing cattle, the time since the last grazing event t_{graz} [days] and the density of cattle in the parcel D_{cow} [cows ha^{-1}] averaged over the last 2, 5, 10, 15, 20, 25, 30 days were tested as predictor variables. For taking into account the influence of slurry and synthetic fertilizer applications, we used categorical variables by attributing time windows of 20, 25, 30, 40, 50-day length after slurry application (Slu) and 10, 15, 20-day length after synthetic fertilizer application (SynF). Pearson correlations identified no high correlations ($\geq$ 0.7) among numeric predictor variables.

For model fitting and validation, our dataset was separated into a training dataset (75 % of data) and a test dataset (25 % of data). This data splitting and the following RF model tuning was performed 10 times for each predictor configuration. The RF algorithm was run via the *train* function (with method *rf*) in the R package *caret*. In this process, the effect of the tuning parameter *mtry* (number of randomly selected predictors at each cut in the tree) was evaluated and the optimal value of 4 was chosen. Accounting for the computation time, we selected a five-fold cross-validation with five repetitions as resampling procedure. The *train* function chose the model with the best performance based on the coefficient of determination (R^2), root mean squared error (RMSE) and mean absolute error (MAE). Different RF models were trained by testing various predictor variable combinations and by using various time intervals for variables P, D_{cow}, Slu and SynF (see above). RF models were validated by the testing dataset to examine the predictive ability using RMSE and R^2.

The relative importance of predictor variables in the final RF model was derived via the *varImp* function of the *caret* package. Furthermore, we used partial dependence plots (R package *pdp*) to visualize the relationship between the outcome and single predictors while accounting for the average effect of the other predictors.

2.5. Flux partitioning

In addition to the gap-filling of measured N_2O fluxes, the final trained RF model was used to disaggregate the gap-filled fluxes $F(N_2O)_{total}$ into three different emission sources: background $F(N_2O)_{bg}$, fertilizer $F(N_2O)_{fertil}$ and excreta $F(N_2O)_{excreta}$:

$$F(N_2O)_{total} \equiv F(N_2O)_{bg} + F(N_2O)_{fertil} + F(N_2O)_{excreta} \quad (3)$$

This was done stepwise in the following way:

1. $F(N_2O)_{bg}$ is defined as the flux not affected by N applications via fertilizer or cattle excreta. Thus, it was calculated with the RF model by setting the management related predictor variables $t_{graz} = 150$ d, $D_{cow} = 0$ and categorical variables Slu and SynF to "no" management.
2. The sum $F(N_2O)_{bg} + F(N_2O)_{excreta}$ not affected by fertilizer applications was calculated for $t_{graz} \leq 60$ d by setting categorical variables Slu and SynF to "no" management. Consequently, $F(N_2O)_{excreta}$ was obtained by subtracting the background flux.
3. $F(N_2O)_{fertil}$ was calculated for respective time windows after fertilisation by rearranging Eq. (3).

$F(N_2O)_{excreta}$ was calculated from the first grazing event in spring to 60 days after the last grazing event in autumn (around the end of December). Literature has shown that average $F(N_2O)_{excreta}$ decrease with time after excreta deposition, e.g. exponentially for cattle urine emissions as found in Voglmeier et al. (2019). For our flux partitioning, we assume that no $F(N_2O)_{excreta}$ occur after 60 days of the last grazing event. In the remaining part of the dormant season (January to March), fluxes arising through the subtraction of $F(N_2O_{bg})$ were assigned as "non-attributed" fluxes.

2.6. N input to pasture and calculation of EFs

N input mainly occurred via excreta of grazing cattle during the grazing season and via several fertilizer applications (slurry and

Table 2
Overview of grazing related parameters (average ± standard deviation) used to calculate the excreta N deposited on the investigated pasture parcels P1 and P3 during grazing periods.

Parameter	Year 1	Year 2	Year 3
Number of grazing days [d yr^{-1}]	45 (P1); 48 (P3)	66	89 (P1); 85 (P3)
Total grazing time [h yr^{-1}]	240 (P1); 271 (P3)	346 (P1); 399 (P3)	734 (P1); 707 (P3)
Grazing time [h d^{-1}]	5 ± 1	5 ± 2	8 ± 3
Number of cattle per grazing parcel	20 ± 1	17 ± 2	16 ± 0
Milk N yield [g $cow^{-1}d^{-1}$]	164 ± 7	153 ± 11	165 ± 13
Cattle live weight [kg]	695 ± 62	725 ± 61	737 ± 79
Net energy demand [MJ $cow^{-1}d^{-1}$]	131 ± 4	129 ± 5	130 ± 5
Energy fed in barn	80 ± 18	93 ± 20	107 ± 16
Energy fed in pasture	51 ± 17	37 ± 19	23 ± 16
N intake [g $cow^{-1}d^{-1}$]	564 ± 57	531 ± 52	506 ± 63
In barn	298 ± 69	350 ± 89	386 ± 46
On pasture	266 ± 84	180 ± 82	120 ± 80
Excreta N [g $cow^{-1}d^{-1}$]	391 ± 53	369 ± 42	335 ± 54

synthetic fertilizers). Slurry and synthetic fertilizer application rates of N ranged from 31 to 69 kg ha^{-1} and 20 to 30 kg ha^{-1}, respectively (Table 1).

For calculating the amount of N excreted by grazing cattle, a cattle N budget approach was used (Table 2). The net energy requirement per cow and day was calculated based on the Swiss feeding recommendations and nutrient tables for ruminants described by Arrigo et al. (1999) as a function of body weight and the energy corrected milk (ECM). To calculate ECM, the milk yield was measured continuously, while the milk was analysed for fat, protein, and lactose content once per month. The cattle body weights were measured 2–6 times per season. The fodder in the barn mainly consisted of hay, maize silage and grass silage, whose characteristics, like dry matter content, energy and crude protein contents, were measured annually while feed intakes in the barn were recorded per herd and day. The N content of the pasture grass was measured every two weeks. The feed intake during grazing was calculated as the difference between the net energy requirement of the cattle and fed energy in the barn. Subsequently, the excreta N [kg $cow^{-1}d^{-1}$] could be estimated by subtracting the total milk N and N in live weight growth from the total fodder N uptake. The excreta N deposited on the pasture [kg $cow^{-1}d^{-1}$] was calculated proportional to the length of grazing recorded through webcams at the pasture side.

The N_2O emission factor EF_3 for cattle excreta was calculated for each year by cumulating all related emissions $\sum F(N_2O)_{excreta}$ divided by the total amount of N applied via cattle excreta $\sum I_{N-excreta}$ (both in units of kg N ha^{-1} yr^{-1}).

$$EF_3 = \frac{\sum F(N_2O)_{excreta}}{\sum I_{N-excreta}} \quad (4)$$

2.7. Uncertainty estimation of yearly emissions and EF_3

Assuming that the data gaps and their filling represents the main error source, the uncertainty of the yearly cumulative emissions for $F(N_2O)_{total}$ and $F(N_2O)_{excreta}$ was estimated from the differences between yearly sums derived by RF using high quality (qc0) fluxes and the respective results including fluxes of the medium quality flag (qc0 plus qc1) with different gap fractions.

The uncertainty of EF_3 was calculated by combining the uncertainty of yearly excreta fluxes, the uncertainty of the cattle N budget approach (15 % according to Voglmeier et al. 2018), and the uncertainty linked to the assumption of a uniform temporal deposition of excreta during the day (40 %; obtained from Draganova et al. (2016) and Aland et al. (2002)) using Gaussian error propagation.

2.8. Driver analysis

The RF algorithm applied in this study provides partial dependence plots (PDPs), which display the effect of single predictor (driver) variables on measured $F(N_2O)$ while holding all other predictor variables constant. They can provide a good general survey of the influence of the individual predictors. However, they do not provide suitable functional relationships nor interpretable insights in the potential interactions between the drivers and their effect on specific source related fluxes. We therefore performed regression analyses to quantify the relationship of $F(N_2O)$ with environmental predictor variables. In a first step, PDPs of the trained RF model were inspected and generalized additive models (GAM; *mgcv* package in R) were fitted. GAMs offer a high flexibility by combining multiple smooth functions of predictor variables and offer restrictive interpretability like the dimension of the basis, p-values of predictors and R^2, but in a non-parametric way. Linear and non-linear models were fitted for various predictor combinations and without specifying a particular shape a-priori. For selecting the final optimum regression model, model outputs were compared by the Akaike information criterion (AIC) and R^2. Furthermore, all predictor coefficients had to be significant.

2.9. Ancillary chamber flux measurements

Chamber flux measurements were performed from July 2020 to September 2022 (during the grazing season) in ten experiments on grazing and fertilization exclusion areas on the same field site as published in Barczyk et al. (2023). An opaque manual chamber of 0.8 m × 0.8 m × 0.5 m was placed on artificially applied urine patches and untreated control areas for 120–130 s. The fluxes were calculated by the 'Hutchinson and Mosier regression (HMR)' according to Pedersen et al. (2010). A more detailed description on the chamber experiments can be found in Barczyk et al. (2023). Only background chamber fluxes were used in this study for validation purposes.

3. Results

3.1. Environmental conditions and measured ec fluxes

During the experiment (April 2020 to April 2023), the soil temperature in 50 mm depth ranged from 0 to 28 °C (Fig. 2). In the winter months (December to February), the average soil temperature was between 2.5 and 4 °C. The total precipitation per year was between 1008 mm and 1351 mm, close to the long-term average (2009–2019) of 1124 mm (MeteoSwiss 2022). On average, the precipitation sum of the summer trimester (437–740 mm) tended to be higher than for winter (257–526 mm), spring (105–419 mm) and autumn (138–363 mm). The monthly precipitation sum was lowest in March 2022 and February 2023 with just 23 mm and 29 mm. The highest monthly precipitation of 373 mm was observed in July 2021, whereas in July 2020 and July 2022 it was only 77 mm and 79 mm. Hence, WFPS of the soil at 5 cm depth stayed below 0.4 in summer 2022 for over one month. In spring, summer and autumn, the WFPS generally showed large variations, ranging from 0.3 to 1.0 while it stayed more stable during the winter (0.72–1.0).

The majority of measured EC N_2O fluxes (87 %) were smaller than 1 g N_2O-N ha^{-1} h^{-1}. Higher N_2O emissions (up to 19 g N_2O-N ha^{-1} h^{-1}) were measured after slurry application, and during the grazing season (April to October) following precipitation events. However, N_2O fluxes > 1 g N_2O-N ha^{-1} h^{-1} also occurred during the winter periods when air temperatures were smaller 0 °C.

3.2. Quality filtering of flux data and performance of RF

Two quality filters for measured N_2O flux data were tested for training the RF model: (i) using only high quality data with flag qc0 and (ii) using high and medium quality data with flags qc0 and qc1. For this comparison, the same training and test data were used. The data coverage of qc01 data (60 %) was considerably higher than using solely qc0 data (38 %). However, the performance of the RF (based on the R^2 and RMSE between predicted and observed values of the training and test data) was better for the qc0 data (Table 3). In addition, the RF trained by qc01 data and consequent flux partitioning yielded unrealistically high $F(N_2O)_{bg}$ in winter that were twice as high as the observed $F(N_2O)_{total}$. We therefore decided to use only qc0 data for the evaluation of N_2O flux data in this study.

Secondly, we had to decide whether to use two separately trained RF models for the fluxes of the two grazing parcels P1 and P3 or to train only one combined RF model for both parcels. A separate RF training for P1 and P3 implied a very low data availability of 23 % and 15 % (qc0), and the corresponding RF model performance was worse compared to the combined RF training. In periods with frequent wind change (SW to NE and vice versa), the separately trained RFs showed similar predictions like the combined RF training (not shown here). In periods with one dominant wind direction, however, visual inspections of the data showed a better performance of the combined RF training. Therefore, the combined RF model was used for further data analysis in this study.

According to the error statistics (R^2 and RSME), the overall performance of RF was the best when using the following predictor variable

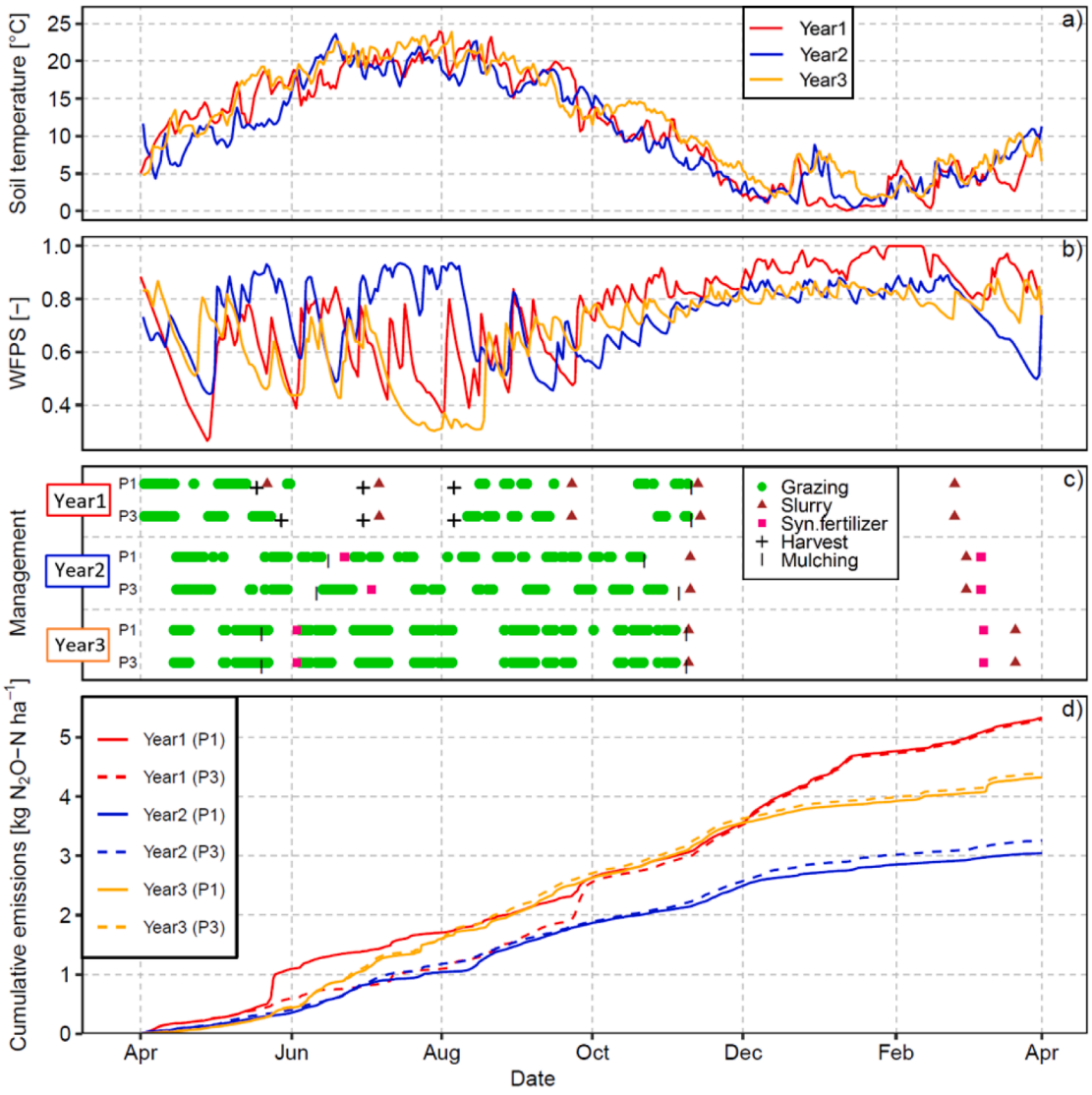

Fig. 2. Environmental conditions, management and N_2O emissions for the tree study years (1 April – 31 May each): (a) soil temperature at 50 mm depth; (b) water-filled pore space at 50 mm soil depth; (c) timing of grazing and other management operations on pasture parcels P1 and P3; (d) cumulative N_2O emissions of the parcels P1 and P3 for the three years.

Table 3
Performance of the random forest (RF) model trained by qc0 and qc01 flux data in predicting measured fluxes of the 25 % test set and in predicting all measured fluxes. Average coefficient of determination (R^2) in percentage and root mean square error (RMSE) in g N_2O-N ha^{-1} h^{-1} plus standard deviation of ten repetitions are shown.

Data used for RF training	Predicted vs 25 % test set				Predicted vs all data			
	qc0		qc01		qc0		qc01	
	R^2	RMSE	R^2	RMSE	R^2	RMSE	R^2	RMSE
qc0	88 ± 1	0.27 ± 0.05	73 ± 1	0.38 ± 0.02	96 ± 1	0.19 ± 0.01	83 ± 0	0.33 ± 0.00
qc01	88 ± 2	0.29 ± 0.03	75 ± 2	0.36 ± 0.02	95 ± 1	0.18 ± 0.04	91 ± 2	0.24 ± 0.03

combination: WFPS, T_s (soil temperature), P (precipitation cumulated over the last 6 h), t_{graz} (days since the last grazing), D_{cow} (density of cattle in the pasture averaged over the past 20 days), Slu (categorical: 0–50 days after slurry application) and SynF (categorical: 0–15 days after synthetic fertilizer application). The frequency distributions of the observed data of these predictor variables are shown in Supplementary Fig. S1. The average R^2 and RMSE (± standard deviation) of the final trained RF model were 0.96 (± 0.01) and 0.19 g N_2O-N ha^{-1} h^{-1} (± 0.01) for the whole dataset, whereas 0.88 (± 0.01) and 0.27 g N_2O-N ha^{-1} h^{-1} (± 0.05) for the 25 % test data, respectively (Table 3).

The RF identified WFPS and T_s as the most important variables (>55 % %IncMSE: decrease of model accuracy when leaving a variable out) for predicting N_2O fluxes, whereas the importance of predictor variables P, t_{graz} and Slu was 40–50 %, and importance of variables SynF and D_{cow} was 15–30 % (Supplementary Fig. S2). The partial dependence plots (PDPs) of the RF, showing the relationship between the N_2O fluxes and single predictors while keeping a constant average effect of the other predictors, can be found in the Supplementary Fig. S3.

3.3. *Cumulative fluxes and contribution of individual emission sources*

The cumulative N_2O emissions resulting from the gap-filled EC fluxes of the three study years were similar for the two parcels P1 and P3 (Fig. 2d). Total annual fluxes (± 95 % confidence interval) were approximately 5.3 ± 0.8 kg N_2O-N ha^{-1} yr^{-1} in year 1, 3.1 ± 0.5 kg N_2O-N ha^{-1} yr^{-1} in year 2 and 4.4 ± 0.7 kg N_2O-N ha^{-1} yr^{-1} in year 3. Also, the temporal evolution of the cumulative emissions was similar for both parcels in year 2 and year 3. In May to September of year 1, though, the

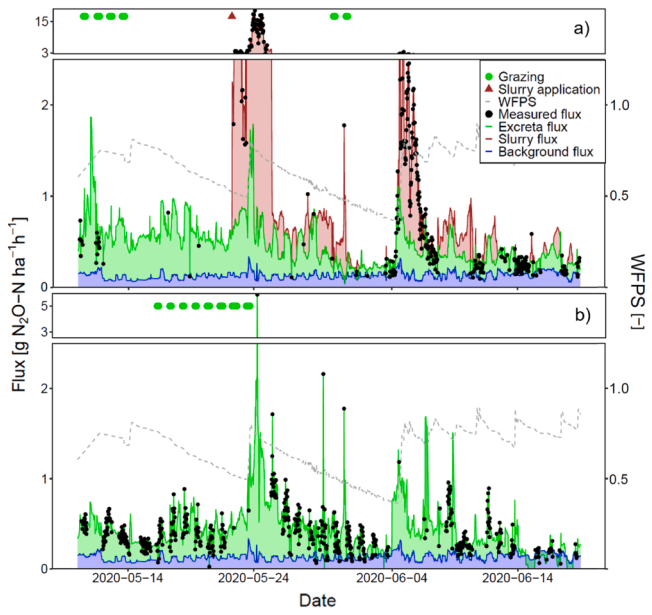

Fig. 3. Exemplary time series of the partitioning of gap-filled fluxes into the emission sources background, grazing related emissions and slurry emissions for the parcels P1 (a) and P3 (b) for a 5-week period in summer 2020. The black points indicate the measured fluxes, the green points the grazing events and the brown triangle shows the timing of slurry application.

temporal evolution was different due to high fluxes after an additional slurry application on P1. In September after another slurry application (conducted on both parcels), the fluxes were higher for P3 so that the cumulative curves of the two parcels were harmonized for the remaining time of year 1.

The partitioning of $F(N_2O)_{total}$ into the emission sources (background, cattle excreta and fertilizer), as explained in the Methodology section, is illustrated for an exemplary five-week period in Fig. 3. $F(N_2O)_{bg}$ values were generally identical for the two parcels because of the use of a combined RF model and the identical values of the environmental predictor variables (WFPS, T_s, P); for the entire experiment, they ranged from 0 to 0.9 g N_2O-N ha^{-1} h^{-1}. For $F(N_2O)_{excreta}$ and F

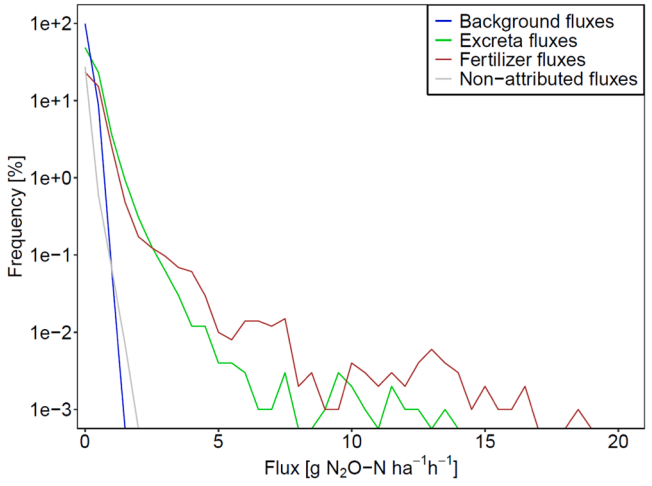

Fig. 4. Frequency distribution of positive half-hourly N_2O fluxes in different categories (background, cattle excreta, fertilizer and non-attributed) obtained by RF flux partitioning for parcels P1 and P3 for the three study years (total data points: 105,120, bin width: 0.5 g N_2O-N ha^{-1} h^{-1}).

$(N_2O)_{fertil}$ also 95 % of data were between 0.0 and 1.0 g N_2O-N ha^{-1} h^{-1}, but the rest ranged up to 13 and 19 g N_2O-N ha^{-1} h^{-1}, respectively (Fig. 4).

Fig. 5 shows the contribution of individual emissions sources to $F(N_2O)_{total}$ over the whole time series.

The contribution of $F(N_2O)_{bg}$ to the cumulative yearly N_2O emissions was similar over the years (Fig. 6) with 1.3 to 1.5 kg N_2O-N ha^{-1} yr^{-1} (27–46 % of total yearly emissions). In year 1, 40 % of the emissions were attributed to the application of fertilizers, and 30 % to the excreta of grazing cattle. In year 2 and year 3, the contribution of fertilizers was smaller with 15 %−19 %. Instead, cattle excreta accounted for 43 %−51 % of the total emissions. In all three years, cumulative $F(N_2O)_{excreta}$ were slightly higher for P3 than for P1. About 3–5 % of the total yearly emissions (derived in the non-grazing period starting six weeks after the last grazing event in autumn to the first grazing event in spring) could not be attributed to one of the emission sources: background, cattle excreta or fertilizer applications (see Methodology).

Yearly cumulative $F(N_2O)_{excreta}$ (± 95 % confidence interval) ranged from 1.3 ± 0.4 kg N_2O-N ha^{-1} yr^{-1} to 2.3 ± 0.7 kg N_2O-N ha^{-1} yr^{-1}. Excreta N inputs ranged from 70 ± 27 kg ha^{-1} yr^{-1} to 210 ± 80 kg ha^{-1} yr^{-1} giving an average EF_3 of 1.1 ± 0.5 % (Fig. 7). EF_3 values were highest in year 1 with 2.1 ± 1.0 % and 1.5 ± 0.7 %, followed by year 3 with 1.3 ± 0.6 % and 1.1 ± 0.5 %, and year 2 with 1.2 ± 0.6 % and 0.8 ± 0.4 % for parcels P1 and P3, respectively.

3.4. Functional relationships with driver variables

In order to estimate the effect of driver variables on total or partitioned fluxes, analytical regression functions were parametrised as described in Section 2.7. In a first step, PDPs of the RF model (Supplementary Fig. S3) were inspected displaying the effect of single predictor (driver) variables on measured $F(N_2O)_{total}$, while holding all other predictor variables constant. According to the variable importance plot (Supplementary Fig. S2), WFPS and T_s were the most important predictor variables in our RF model. For predictor variable WFPS (at values > 0.4), the PDP shows an optimum curve giving highest outcome at around 0.7. For low WFPS < 0.4, the effect on measured $F(N_2O)_{total}$ increased again in an unexpected way. The PDP for predictor variable T_s (> 3 °C) shows a continuous increase of the measured $F(N_2O)_{total}$ with T_s until reaching a plateau at 25 °C. At $T_s \leq 3$ °C, another steep increase of $F(N_2O)_{total}$ is shown, which indicates a different process dominating in this temperature range.

For the main environmental parameter range $T_s > 3$ °C and WFPS $>$ 0.4 (81 % of data), $F(N_2O)_{bg}$ could be described as a combined polynomial function of WFPS [%] and a linear function of T_s [°C] (Table 4, Eq. (5a)). The function shows smallest values close to zero at T_s close to 3 °C and WFPS of 0.4 or 1, and highest values around 0.3 g N_2O-N ha^{-1} h^{-1} at $T_s = 26$ °C and WFPS = 0.7. We found no suitable regression model that could parametrize the dependency of $F(N_2O)_{fertil}$ and $F(N_2O)_{excreta}$. For all tested regression models, the R^2 was < 0.15. For very complex models (e.g. with multiple interactions) R^2 was up to 0.30, however prone to overfitting and more difficult to interpret.

Since the inspection of the RF PDPs (Supplementary Fig. S3) showed an unexpected behaviour for low soil temperatures (cold season: $T_s \leq 3$ °C and WFPS > 0.7) and very dry conditions (summer drought: WFPS $<$ 0.4 and $T_s > 15$ °C), the data in these parameter ranges were analysed in more detail and parameterised separately (Table 4). The summer drought during six weeks in year 3 with WFPS < 0.4 and $T_s > 15$ °C (Fig. 2a,b) is unique within our dataset, while conditions with low soil temperatures ($T_s \leq 3$ °C and WFPS > 0.7) occurred sporadically or sometimes frequent (one month in year 1) in winter. Due to a comparably low data availability of measured fluxes during these special environmental conditions (n = 1556 in the cold season; n = 571 in the summer drought), we assume that the disaggregation of $F(N_2O)_{total}$ into the individual emission sources by RF is less confident. Therefore, the driver analysis was performed by using measured $F(N_2O)_{total}$.

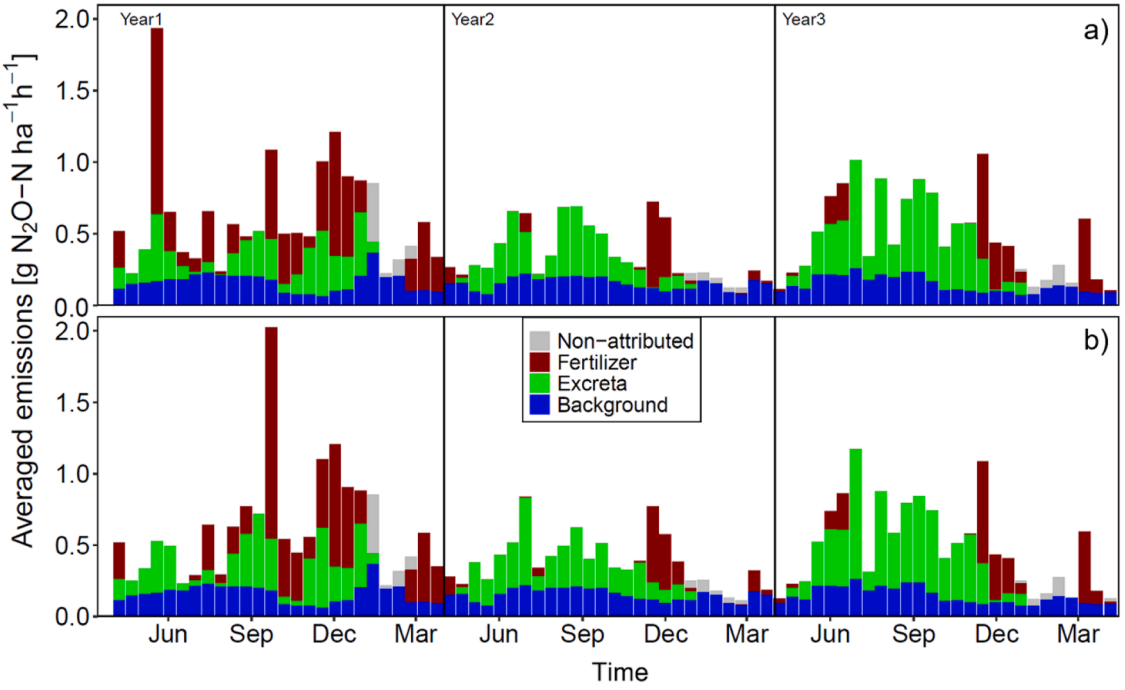

Fig. 5. Contribution of individual emission sources (Background, excreta and fertilizer) to the total N_2O emissions over the three years of experiment for parcels P1 (a) and P3 (b). Emissions are averaged over two weeks.

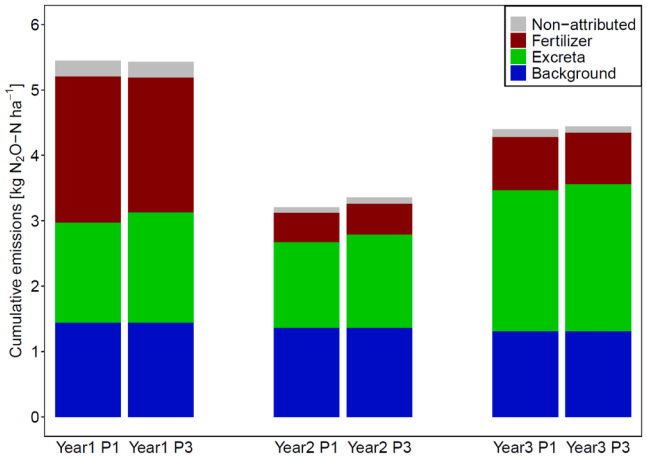

Fig. 6. Contribution of the different emission sources (background, grazing and fertilizer) to the yearly cumulative N_2O emissions as obtained by the RF flux partitioning for the three study years and the two pasture parcels P1 and P3.

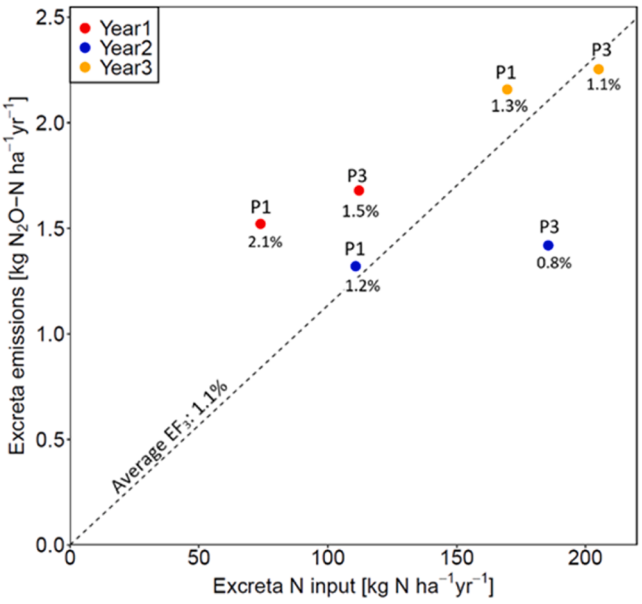

Fig. 7. Yearly excreta N_2O emissions plotted against yearly excreta N inputs of the two parcels (P1 and P3). Resulting EF_3 values and average EF_3 (linear regression slope by setting y-intercept to zero) are shown in the plot.

In the cold season ($T_s \leq 3$ °C and WFPS > 0.7), peak $F(N_2O)_{total}$ up to 3.9 g N_2O-N ha^{-1} h^{-1} (Supplementary Figure S4) occurred that were parametrised as an exponential decay function of T_s (Eq. 5b). Since T_s at 50 mm depth generally did not show negative values indicating freezing, the air temperature was included in the analysis to better represent the conditions at the soil surface. In the period of highest cold season emission values (Fig. 8) in February 2023, diurnal peaks occur when the air temperature gets positive after nights with clearly negative values.

For the summer drought period (WFPS < 0.4 and T_s > 15 °C) displayed in Fig. 9, measured $F(N_2O)_{total}$ peaked up to 13.9 g N_2O-N ha^{-1} h^{-1}, while WFPS showed almost no variations. However, N_2O emissions exhibited a linear dependence on the cumulative precipitation over the last six hours (P) and the time in days since the last grazing (t_{graz}).

4. Discussion

4.1. Gap-filling and annual emissions

After gap-filling, the cumulative N_2O emissions were determined to be 5.3 ± 0.8, 3.1 ± 0.5 and 4.4 ± 0.7 kg N_2O-N ha^{-1} yr^{-1} (Fig. 6), which are lower than the global IPCC default value of 8 kg N_2O-N ha^{-1} yr^{-1} for grazed pasture (de Klein et al. 2006), and in the lower range of reported values of 2 to 15 kg N_2O-N ha^{-1} yr^{-1} (Luo et al. 2008; de Klein et al. 2010;

Table 4
Equations to parametrize background and measured N_2O emissions ($F(N_2O)_{bg}$ and $F(N_2O)$total in units of g N_2O-N ha^{-1} h^{-1}) at different environmental conditions. The following predictor variables were used: water-filled pore space (WFPS), soil temperature (T_s), time in days since the last grazing (t_{graz}) and cumulated precipitation over the last six hours (P).

Parameterized flux	Environmental conditions	Equation	
$F(N_2O)_{bg}$	$T_s > 3$; WFPS > 0.4 (growing season)	$1.10\ WFPS^2 - 1.01\ WFPS^3 + 0.012\ T_s - 0.15$ ($R^2 = 0.45$, $p < 0.0001$)	(Eq. 5a)
$F(N_2O)_{total}$	$T_s \leq 3$; WFPS > 0.7 (cold season)	$1.54\ \exp^{(-1.88\ T_s)} + 0.14$ ($R^2 = 0.84$, $p < 0.0001$)	(Eq. 5b)
$F(N_2O)_{total}$	WFPS ≤ 0.4; $T_s > 15$ °C (summer drought)	$0.36\ P - 0.088\ t_{graz} + 0.82$ ($R^2 = 0.30$, $p < 0.0001$)	(Eq. 5c)

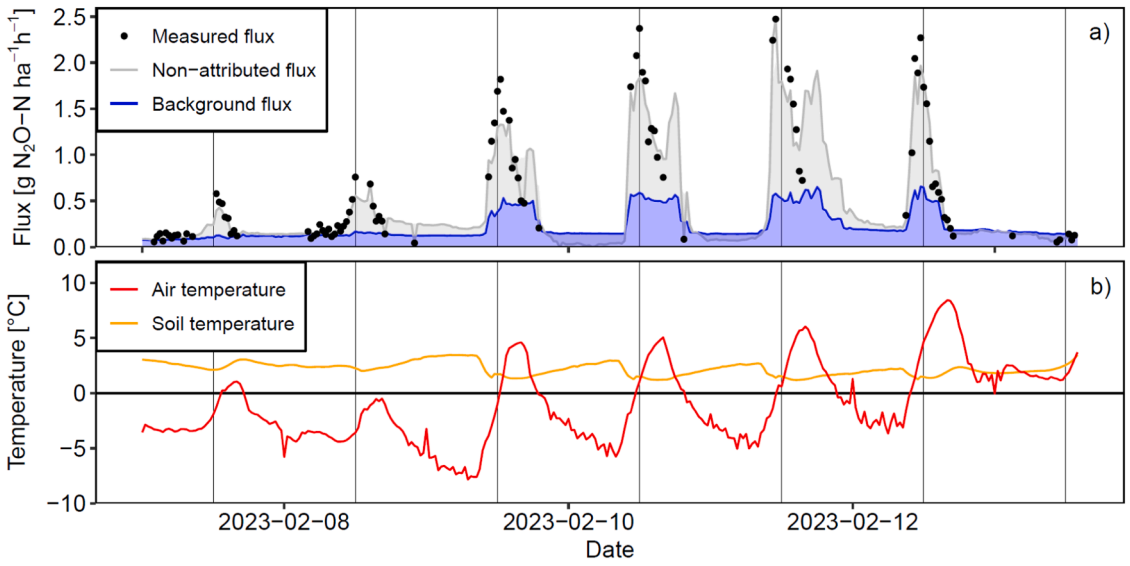

Fig. 8. Exemplary N_2O flux time series (a) with peak emissions during winter together with air temperature (b), and vertical lines at midday. Measured and predicted/partitioned N_2O fluxes are shown combined for the two parcels P1 and P3. The air temperature measured in 2 m height is plotted together with the soil temperature in 50 mm depth.

Luo et al. 2019). Voglmeier et al. (2020) found similar emissions of 3.7–3.8 kg N_2O-N ha^{-1} yr^{-1} at a dairy pasture in Western Switzerland.

In consistency with previous studies that used RF for the gap-filling of EC $F(N_2O)$, our results showed a good performance of the RF model in $F(N_2O)$ gap-filling (Table 3, Fig. 3); it was able to capture the highly variable temporal evolution of $F(N_2O)$ from low fluxes (close to zero) up to pulse fluxes as large as 19 g N_2O-N ha^{-1} h^{-1}.

Due to a separate flux gap-filling for parcels 1 and 3, and thus longer gaps of up to two weeks, linear interpolation or running average were not able to capture the temporal development of N_2O fluxes comparably to the RF (not shown here). Similarly, Taki et al. (2019) and Bigaignon et al. (2020) showed a better statistical score and a better prediction of the N_2O flux variability for ANN compared to linear interpolation for cropland. However, in our study yearly cumulated fluxes were similar (maximum deviation of 10 %) when applying a running average (with adaptive window size to always include 12 data points) to gap-fill the F (N_2O) time series.

Besides Goodrich et al. (2021), there are no reports in literature comparing different ML algorithms for EC N_2O gap-filling. Kim et al. (2019), however, compared three ML algorithms (ANN, RF, and support vector machine) for the gap-filling of CH_4 fluxes showing the best scores for RF gap-filling. Kim et al. (2019) even suggested using RF as standard gap-filling method for CH_4 fluxes, because RF not only showed the best performance among different ML algorithms, but it was also found to be more straightforward to use and less sensitive to overfitting compared to ANN, for instance.

In our study, the RF was trained by best-quality data (qc0: 38 % coverage), but test calculations with less strict quality filtering (qc01: 60 % coverage) were also made. Interestingly, for both input datasets, the trained RF models were better in predicting qc0 data than in predicting qc01 data (Table 3). In addition, the predictions of qc0 trained RF and qc01 trained RF were highly correlated ($R^2 = 0.95$) in spite of different data availabilities. Thus, a higher data availability (by including qc1 data) did not yield a better performance of the RF. Thus, we conclude that qc1 data were too noisy and thus not useful for the RF training. The 0–1–2 quality flag approach of Mauder and Foken (2004) has often been used for GHG fluxes, and typically quality flags 0 and 1 are applied for the analysis (Fuchs et al. 2018; Wecking et al. 2020; Goodrich et al. 2021; Xie et al. 2022). For our dataset, the average (systematic) difference between cumulative yearly emissions derived by RF gap-filling using solely qc0 data and using qc01 was 16 % on average. Yet, the choice of acceptable quality flag values for data filtering might have stronger effects on the results, e.g. when using regression methods that, in contrast to the RF, react more sensitive to noisy data.

4.2. *Flux partitioning by random forest*

Flux partitioning, i.e. the disaggregation of gap-filled EC fluxes into the emissions sources (background, cattle excreta, fertilizer) is necessary to calculate EFs of different emission sources. The EC flux partitioning by RF does not require additional chamber experiments with artificially applied excreta patches, but merely relies on observed field-scale fluxes of the real pasture. Yet, chamber measurements conducted at the same site and in the same time period (Barczyk et al. 2023) support the results of the partitioning showing background fluxes in a similar range as derived from EC measurements (Fig. 10). The obtained results for $F(N_2O)_{bg}$, $F(N_2O)_{fertil}$ and $F(N_2O)_{excreta}$ also were comparable to available literature reports using chambers (Voglmeier et al. 2020; Wecking et al. 2020; Murphy et al. 2022). Cumulative $F(N_2O)_{bg}$ of 1.3 to 1.5 kg N_2O-N ha^{-1} yr^{-1} were close to the global mean of 1.8 kg N_2O-N ha^{-1} yr^{-1} quantified in a meta-analysis by Kim et al. (2013). The cumulative $F(N_2O)_{fertil}$ corresponds to an average EF for fertilizer applications of 0.7 ± 0.4 %

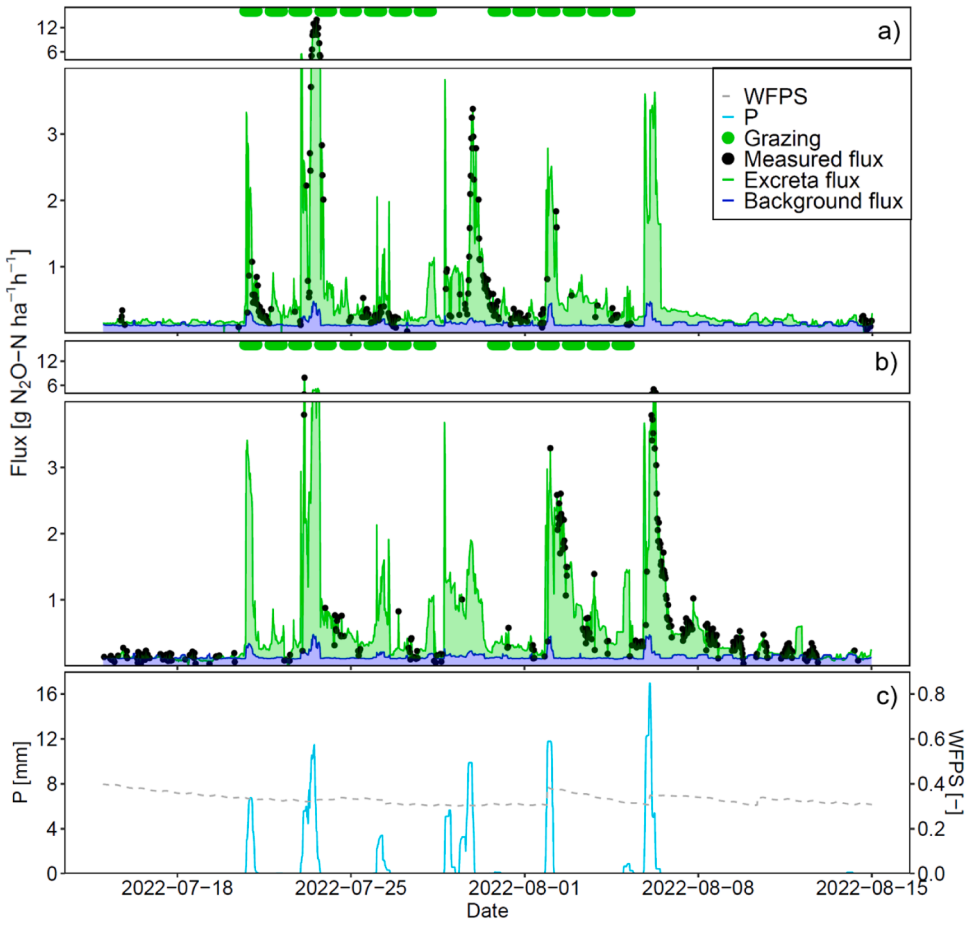

Fig. 9. Time series of measured and partitioned N_2O fluxes during the drought period in year 3 with peak N_2O emissions in parcel P1 (a) and P3 (b) occurring after precipitation (c). The parameter P represents precipitation cumulated over the past six hours.

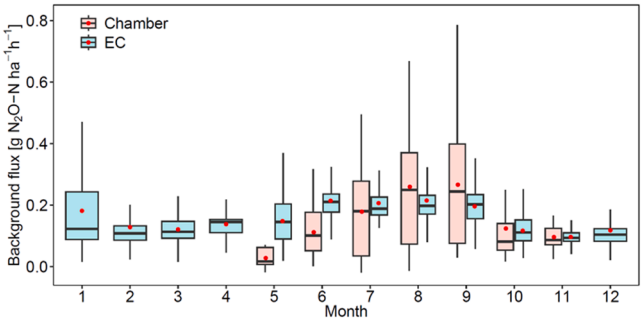

Fig. 10. Boxplots including arithmetic mean (red circle) of background fluxes measured by a manual chamber and calculated from partitioning of eddy covariance (EC) derived fluxes per month of the year.

(mean ± standard deviation) and is reasonably close to the global default EF_1 of 1 % suggested by the IPCC (IPCC 2019). The contributions of cumulative $F(N_2O)_{fertil}$ and $F(N_2O)_{excreta}$ can vary significantly depending on the grazing system and management practices, as seen in our study comparing year 1 with more slurry applications and less grazing to year 2 and year 3 with less slurry applications and more grazing events.

However, it is important to note that for the flux gap-filling and partitioning by RF in the present study, assumptions had to be made. N inputs via atmospheric deposition, harvest residues and biological fixation (as suggested by the IPCC) were not explicitly considered in our study and are expected to be small compared to cattle excreta and fertilizer N inputs (Kosonen et al. 2019; Schmid et al. 2001). Related N_2O emissions are included in $F(N_2O)_{bg}$. Furthermore, by using categorical variables for the time periods possibly affected by fertilizer applications (differentiated between synthetic fertilizer and slurry), the effect of the N application rate for each individual fertilizer application was not considered as a predictor variable in the RF model set up, although a direct (linear) effect on the N_2O emission is generally assumed (van Groeningen et al. 2004). In our study, the N application rate (Table 1) was generally higher and more variable for slurry (35–69 kg N ha^{-1}) than for synthetic fertilizer (20–30 kg N ha^{-1}) because, according to the Swiss guidelines for integrated management, 67 % more N can be applied as slurry compared to synthetic fertilizers. We set the time span of possible slurry and synthetic fertilizer emissions to 0–50 and 0–15 days after application, respectively, based on visual inspection of our data and promoted by a better performance of the RF compared to other time spans (see Methodology section). Many studies showed a major portion of cumulative fertilizer emissions occurring within the first two weeks, typically instantaneously after application and in a distinct peak (e.g. van Groeningen et al. 2004; Schils et al. 2008). Nevertheless, the persistence of fertilizer related emissions can vary greatly, e.g. up to 150 days (van Groeningen et al. 2004) for slurry. On the other hand, some studies even recorded no distinct increase of emissions after fertilizer application (Schils et al. 2008). For our study, we cannot fully rule out the possibility that $F(N_2O)_{fertil}$ lasted longer than the used time spans, e.g. into the spring, as high emission occurred at low temperatures (especially in year 1) in January and February assigned as “non-attributable”.

Non-attributed fluxes were calculated like $F(N_2O)_{excreta}$ (Sect. 2.5) for winter/spring periods presumably not affected by grazing ($t_{graz} > 60$

d) nor fertilizer applications by subtracting $F(N_2O)_{bg}$ from $F(N_2O)_{total}$. Since their annual contribution was relatively small, we did not assign them to one of the other flux categories. They may be regarded as part of the partitioning uncertainty.

4.3. Reliability of EF_3 values

The average EF_3 value of 1.1 ± 0.5 %, derived in our study (Fig. 7), is between the new IPCC EF_3 value for wet climates of 0.6 % and the old one of 2.0 %. Furthermore, it is higher than the estimated value of about 0.5 % quantified in ten chamber trials by Barczyk et al. (2023) at the same field site.

Based on literature reports, EC fluxes generally tend to be higher than chamber fluxes (Jones et al. 2011; Wang et al. 2013; Wecking et al. 2020). We suppose that the EC technique gives a more reliable picture on pasture $F(N_2O)_{total}$ than chamber measurements as it measures in a higher temporal resolution and is able to cover the spatial variability of a pasture. Moreover, it relies on real observations. In chamber trials, urine (predominantly as synthetic surrogate solution) commonly has been applied artificially in fenced-out areas of a pasture field (Kool et al. 2006; Murphy et al. 2022; Barczyk et al. 2023), and thus possibly did not affect soil processes equally to real cattle urine patches. Interactions of excreta patches with other influencing factors like the trampling of cattle, fertilizer applications or overlapping excreta patches (Treweek et al. 2016; Maire et al. 2020) can be hardly reproduced in its entirety in chamber trials. Moreover, chamber measurement areas are commonly excluded from grazing and from other N inputs for several months prior to the treatment application. Lastly, $F(N_2O)_{excreta}$ during winter are usually not considered in chamber trials. In this study, we found considerable $F(N_2O)_{excreta}$ and "non-attributable" N_2O fluxes at low soil temperatures during winter (especially in year 1), which should be considered in future studies.

However, the EC technique involves other uncertainties like the need for flux partitioning. Moreover, while excreta N inputs can be controlled and easily quantified in chamber trials, we suppose that the highest uncertainty of EC derived EF_3 values lies in the calculation of the excreta-derived N inputs. This is especially the case for partly day grazing. In our study, the pastoral excreta N input was calculated proportional to the grazing time that was six hours on average. It is unclear whether there is a diurnal cycle of cattle excretion, e.g. a lower excretion frequency at night, as literature reports give non-consistent results (Aland et al. 2002; Draganova et al. 2016). Furthermore, we assume a homogenously distributed application of excreta in the field. As the pasture of our study was part-day grazed and there were no trees or other shadow providing shelters, we assume a low risk of so-called camping areas (except for areas around the standpipes at high T_s in summer) in which excreta patch densities can be elevated (Iyyemperumal et al. 2007; Draganova et al. 2016).

4.4. Dependence on environmental drivers

The temporal variations of $F(N_2O)_{bg}$ during the growing season ($T_s > 3°$) and outside of drought conditions (WFPS > 0.4) could be predicted mainly by WFPS and T_s, concurrently found to be the most important predictors in the RF model. WFPS is known to be a major driver of N_2O emissions as it affects microbial activity by controlling the availability of oxygen and water (Butterbach-Bahl et al. 2013). Literature proposes an optimum curve with maximum values of N_2O production at 0.6–0.8 WFPS (Davidson et al. 1991; Butterbach-Bahl et al. 2013; Congreves et al. 2019) that corresponds to our findings in the driver analysis (Table 4) and to the average effect of WFPS visualized in the PDP of the RF model for WFPS > 0.4 (Supplementary Fig. S3). $F(N_2O)_{bg}$ increased with T_s (also seen in the PDP) and can be explained by enhanced soil microbial activity at higher T_s (Butterbach-Bahl et al. 2013).

During the cold season ($T_s \leq 3$ °C) we observed significant peaks of $F(N_2O)_{total}$ up to 3.9 g N_2O-N ha^{-1} h^{-1}. These peaks might be explained by so called freeze-thaw effects, occurring when a frozen soil thaws and trapped gases including N_2O can be released (Öquist et al. 2004; Wagner-Riddle et al. 2017). In our study, T_s was measured in 50 mm depth and observed minimum values between 0 and 1 °C would not imply a frozen soil. However, surface soil (few mm deep) has a much stronger diurnal variation in temperature than deeper soil layers, and air temperature measured at 2 m height above ground went down to −9 °C suggesting that the soil surface was temporary frozen. Fig. 8 shows as an example that peak $F(N_2O)_{total}$ fluxes occurred in winter during day-time at maximum air temperatures after night-time air temperatures clearly below 0 °C. Koponen et al. (2004) moreover observed peak emissions at T_s close to 0 °C and without previous freezing of the soil. They hypothesized that the low T_s leads to a low microbial population towards a critical point. The decomposition of dead microbial cells would then lead to a sudden increase of substrate availability used by still existing microorganisms causing $F(N_2O)$ peaks. For our study, we suppose that both processes, freeze-thaw effect and the effect explained by Koponen et al. (2004), contributed to peak $F(N_2O)$ at low T_s.

During a drought period in the summer of year 3 with WFPS ≤ 0.4 with occasional grazing, we found distinct peaks of $F(N_2O)_{total}$ that correlated with the predictor variable P. N_2O peaks after rewetting a dry soil were documented by other studies (Leitner et al. 2017; Barrat et al. 2021). Though hardly detected by our soil moisture sensors at 50 mm depth, we suppose that precipitation activated microbial activity in the surface soil. In addition to precipitation, the deposition of excreta in the field entailed up to 17 mm liquid per urine patch and the simultaneous application of excreta N presumably triggered N_2O producing microbial processes (Selbie et al. 2015).

5. Conclusions

We conclude that the RF is a suitable method for the gap-filling and partitioning of EC derived N_2O fluxes. Clearly, a combination of several environmental and management related predictor variables is needed to drive RF models and must be measured accordingly. EC based N_2O flux measurements under real pasture conditions with subsequent RF flux gap-filling and partitioning may particularly improve the quantification of $F(N_2O)_{excreta}$. Real pasture conditions including possible interactions of fertilisers with excreta patches cannot be simulated to the full extent in chamber trials. This may be one reason why the obtained average EF_3 of 1.1 % was higher than estimated by chamber experiments with artificial patches at the same site.

In addition, this study demonstrated that PDPs of a RF model can be used to investigate the influence of single drivers on $F(N_2O)_{total}$. PDPs made it possible to recognize that high $F(N_2O)_{total}$ unexpectedly occurred during a drought period in summer and cold periods in winter. In both cases the soil conditions (drivers) measured at 50 mm depth were insufficient to explain the emission peaks, but inferred moisture and temperature conditions directly at the soil surface may provide a better correlation with the observed N_2O emissions. This issue requires further detailed investigation and suggests temperature and moisture measurements closer to the soil surface.

CRediT authorship contribution statement

Lena Barczyk: Writing – original draft, Visualization, Investigation, Formal analysis. **Johan Six:** Writing – review & editing, Supervision. **Christof Ammann:** Writing – review & editing, Supervision, Project administration, Funding acquisition, Conceptualization.

Declaration of competing interest

The authors declare that they have no known competing financial interests or personal relationships that could have appeared to influence the work reported in this paper.

Acknowledgements

We thank Markus Jocher for substantial help in setting up the field experiment and maintenance of the EC measurements. Furthermore, we thank Sabine Schrade and Michael Zähner for providing cattle specific data. In this context, we thank Daniel Bretscher who helped in calculating the excreta N. This study was funded by the Swiss National Science Foundation (SNF) under the project REFGRASS (Towards Representative N2O Emission Factors for Grazing Systems in Switzerland, Nr. 184797).

Supplementary materials

Supplementary material associated with this article can be found, in the online version, at doi:10.1016/j.agrformet.2024.110278.

References

Ackermann, D., Millet, D.B., Chen, X., 2019. Global estimates of inorganic nitrogen deposition across four decades. Global. Biogeochem. Cycles. 33, 100–107. https://doi.org/10.1029/2018GB005990.

Aland, A., Lidfors, L., Ekesbo, I., 2002. Diurnal distribution of dairy cow defecation and urination. Appl Anim Behav 78, 43–54.

Arrigo, Y., Chaubert, C., Daccord, R., Gagnaux, D., Gerber, H., Guidon, D., Jans, F., Kessler, J., Lehmann, E., Morel, I., Münger, A., Rouel, M., Wyss, U., 1999. Fütterungsempfehlungen Und Nährwerttabellen für Wiederkäuer: Das Grüne Buch, fourt ed. Eidgenössische Forschungsanstalt für Nutztiere, Zollikofen, Switzerland.

Barczyk, L., Kuntu-Blankson, K., Calanca, P., Six, J., Ammann, C., 2023. N_2O emission factors for cattle urine: efect of patch characteristics and environmental drivers. Nutr. Cycl. Agroecosyst. 127, 173–189. https://doi.org/10.1007/s10705-023-10290-0.

Barrat, H.A., Evans, J., Chadwick, D.R., Clark, I.M., Le Cocq, K., Cardenas, L., 2021. The impact of drought and rewetting on N_2O emissions from soil in temperate and Mediterranean climates. Eur. J. Soil. Sci. 72, 2504–2516. https://doi.org/10.1111/ejss.13015.

Beltran, I., van der Weerden, T.J., Alfaro, M.A., Amon, B., de Klein, C.A.M., Grace, P., Hafner, S., Hassouna, M., Hutchings, N., Krol, D.J., Leytem, A.B., Noble, A., Salazar, F., Thorman, R.E., Velthof, G.L., 2021. DATAMAN: a global database of nitrous oxide and ammonia emission factors for excreta deposited by livestock and land-applied manure. J. Environ. Qual. 50, 513–527. https://doi.org/10.1002/jeq2.20186.

Bigaignon, L., Fieuzal, R., Delon, C., Tallec, T., 2020. Combination of two methodologies, artificial neural network and linear interpolation, to gap-fill daily nitrous oxide flux measurements. Agric. For. Meteorol. 291, 108037.

Breiman, L., 2001. Random forests. Mach. Learn. 45, 5–32.

Butterbach-Bahl, K., Baggs, E.M., Dannenmann, M., Kiese, R., Zechmeister-Boltenstern, S., 2013. Nitrous oxide emissions from soils: how well do we understand the processes and their controls? Phil. Trans. R. Soc. B368, 20130122. https://doi.org/10.1098/rstb.2013.0122.

Congreves, K.A., Phan, T., Farrell, R.E., 2019. A new look at an old concept: using 15N2O isotopomers to understand the relationship between soil moisture and N_2O production pathways. Soil 5, 265–274. https://doi.org/10.5194/soil-5-265-2019.

Cowan, N., Levy, P., Maire, J., Coyle, M., Leeson, S.R., Famulari, D., Carozzi, M., Nemitz, E., Skiba, J., 2020. An evaluation of four years of nitrous oxide fluxes after application of ammonium nitrate and urea fertilisers measured using the eddy covariance method. Agric. For. Meteorol. 280, 107812. https://doi.org/10.1016/j.agrformet.2019.107812.

Cutler, D.R., Edwards, T.C., Beard, K.H., Cutler, A., Hess, K.T., Gibson, J., Lawler, J.J., 2007. Random forests for classification in ecology. Ecology. 88, 2783–2792.

edited by: Davidson, E.A., 1991. Fluxes of nitrous oxide and nitric oxide from terrestrial ecosystems, in: microbial production and consumption of greenhouse gases: methane, nitrogen oxides and halomethanes. In: Rogers, JE, Whitman, WB (Eds.), Fluxes of nitrous oxide and nitric oxide from terrestrial ecosystems, in: microbial production and consumption of greenhouse gases: methane, nitrogen oxides and halomethanes. Am. Soc. Microbiol. J Environ. Qual. 23, 211–212. https://doi.org/10.2134/jeq1994.00472425002300010034x.

de Klein, C.A.M., Novoa, R.S.A., Ogle, S., Smith, K.A., Rochette, P., Wirth, T.C., McConkey, B.G., Mosier, A., Rypdal, K., 2006. N_2O emissions from managed soils, and CO_2 emissions from lime and urea application. In: Gytarsky, M., Higarashi, T., Irving, W., Krug, T., Penman, J. (Eds.), 2006 IPCC Guidelines for National Greenhouse Gas Inventories. Intergovernmental Panel on Climate Change (IPCC). Geneva, Switzerland, pp. 11.1–11.54.

de Klein, C.A.M., Eckhard, R., van der Weerden, T., 2010. Nitrous oxide emissions from the nitrogen cycle in livestock agriculture: estimation and mitigation. In: Smith, K.A. (Ed.), Nitrous Oxide and Climate Change. Earthscan, London, pp. 107–142.

Draganova, I., Yule, I., Stevenson, M., Betteridge, K., 2016. The effects of temporal and environmental factors on the urination behaviour of diary cows using tracking and sensor technologies. Precision Agric 17, 407–420.

Du, Y., Ke, X., Li, J., Wang, Y., Cao, G., Guo, X., Chen, K., 2021. Nitrogen deposition increases global grassland N_2O emission rates steeply: a meta-analysis. Catena 199, 105105. https://doi.org/10.1016/j.catena.2020.105105.

Duchicela, S.A., Cuesta, F., Tovar, C., Muriel, P., Jaramillo, R., Salazar, E., Pinto, E., 2021. Microclimatic warming leads to a decrease in species and growth form diversity: insights from a tropical alpine grassland. Front. Ecol. Evol. 9, 672655. https://doi.org/10.3389/fevo.2021.673655.

Feigenwinter, I., Hörtnagl, L., Buchmann, N., 2023. N2O and CH4 fluxes from intensively managed grassland: the importance of biological and environmental drivers vs. management. Sci. Total. Environ. 903, 166389. https://doi.org/10.1016/j.scitotenv.2023.166389.

Fratini, G., Ibrom, A., Arriga, N., Burba, G., Papale, D., 2012. Relative humidity effects on water vapour fluxes measured with closed-path eddy-covariance systems with short sampling lines. Agric. For. Meteorol. 165, 53–63. https://doi.org/10.1016/j.agrformet.2012.05.018.

Fuchs, K., Hörtnagl, L., Buchmann, N., Eugster, W., Snow, V., Merbold, L., 2018. Management matters: testing a mitigation strategy for nitrous oxide emissions using legumes on intensively managed grassland. BG 15, 5519–5543. https://doi.org/10.5194/bg-15-5519-2018.

Goodrich, J.P., Wall, A.M., Campbell, D.I., Fletcher, D., Wecking, A.R., Schipper, L.A., 2021. Improved gap filling approach and uncertainty estimation for eddy covariance N_2O fluxes. Agric. For. Meteorol. 297, 108280. https://doi.org/10.1016/j.agrformet.2020.108280.

Grace, P.R., van der Weerden, T.J., Rowlings, D.W., Scheer, C., Brunk, C., Kiese, R., Butterbach-Bahl, K., Rees, R.M., Robertson, G.P., Skiba, U.M., 2020. Global Research Alliance N_2O chamber methodology guidelines: considerations for automated flux measurement. J. Environ. Qual. 49, 1126–1140. https://doi.org/10.1002/jeq2.20124.

He, S., Wu, J., Wang, D., Xiaodong, He, 2022. Predictive modeling of groundwater nitrate pollution and evaluating its main impact factors using random forest. Chemosphere 290, 133388. https://doi.org/10.1016/j.chemosphere.2021.133388.

IPCC, 2006. In: Eggleston, HS, Buendia, L, Miwa, K, Ngara, T, Tanabe, K (Eds.), 2006 IPCC Guidelines for National Greenhouse Gas Inventories, Prepared by the National Greenhouse Gas Inventories Programme. Published: IGES, Japan.

IPCC, 2019. In: Calvo Buendia, E, Tanabe, K, Kranjc, A, Baasansuren, J, Fukuda, M, Ngarize, S, Osako, A, Pyrozhenko, Y, Shermanau, P, Federici, S (Eds.), 2019 Refinement to the 2006 IPCC Guidelines for National Greenhouse Gas Inventories. Published: IPCC, Switzerland.

Iyyemperumal, K., Israel, D.W., Shi, W., 2007. Soil microbial biomass, activity and potential nitrogen mineralization in a pasture: impact of stock camping activity. Soil. Biol. Biochem. 39, 149–157. https://doi.org/10.1016/j.soilbio.2006.07.002.

Jones, S.K., Famulari, D., Di Marco, C.F., Nemitz, E., Skiba, U.M., Rees, R.M., Sutton, M.A., 2011. Nitrous oxide emissions from managed grassland: a comparison of eddy covariance and static chamber measurements. Atmos. Meas. Tech. 4, 2179–2194. https://doi.org/10.5194/amt-4-2179-2011.

Kim, D-G, Giltrap, D., Hernandez-Ramirez, G., 2013. Background nitrous oxide emissions in agricultural and natural lands: a meta-analysis. Plant Soil. 373, 17–30. https://doi.org/10.1007/s11104-013-1762-5.

Kim, Y., Johnsom, M.S., Knox, S.H., Black, T.A., Dalmagro, H.J., Kang, M., Kim, J., Baldocchi, D., 2019. Gap-filling approaches for eddy covariance methane fluxes: a comparison of three machine learning algorithms and a traditional method with principal component analysis. Glob. Change Biol. 26, 1499–1518. https://doi.org/10.1111/gcb.14845.

Kool, D.M., Hoffland, E., Abrahamse, S.P.A., Van Groenigen, J.W., 2006. What artificial urine composition is adequate for simulating soil N_2O fluxes and mineral N dynamics? Soil. Biol. Biochem. 38, 1757–1763. https://doi.org/10.1016/j.soilbio.2005.11.030.

Koponen, H.T., Flöjt, L., Martikainen, P.J., 2004. Nitrous oxide emissions from agricultural soils at low temperatures: a laboratory microcosm study. Soil. Biol. Biochem. 36, 757–766. https://doi.org/10.1016/j.soilbio.2003.12.011.

Korman, R., Meixner, F., 2001. An analytical footprint model for non-neutral stratification. Boundary-Layer Meteorol 99, 207–224.

Kosonen, Z., Schnyder, E., Hiltbrunner, E., Thimonier, A., Schmitt, M., Seitler, E., Thöni, L., 2019. Current atmospheric nitrogen deposition still exceeds critical loads for sensitive, semi-natural ecosystems in Switzerland. Atmos. Environ. 211, 214–225. https://doi.org/10.1016/j.atmosenv.2019.05.005.

Kroeze, C., Mosier, A., Bouwman, L., 1999. Closing the global N_2O budget: a retrospective analysis 1500–1994. Global Biogeochem. Cycles 13, 1–8. https://doi.org/10.1029/1998GB900020.

Leitner, S., Homyak, P.M., Blankinship, J.C., Eberwein, J., Jenerette, G.D., Zechmeister-Boltenstern, S., Schimel, J.P., 2017. Linking NO and N_2O emission pulses with the mobilization of mineral and organic N upon rewetting dry soils. Soil. Biol. Biochem. 115, 461–466. https://doi.org/10.1016/j.soilbio.2017.09.005.

Levy, P.E., Cowan, N., van Oijen, C.M., Famulari, D., 2017. Estimation of cumulative fluxes of nitrous oxide: uncertainty in temporal upscaling and emission factors. Eur. J. Soil. Sci. 68, 400–411. https://doi.org/10.1111/ejss.12432.

Liang, L.L., Campbell, D.I., Wall, A.M., Schipper, L.A., 2018. Nitrous oxide fluxes determined by continuous eddy covariance measurements from intensively grazed pastures: temporal patterns and environmental controls. Agric. Ecosyst. Environ. 268, 171–180. https://doi.org/10.1016/j.agee.2018.09.010.

Luo, J., Ledgard, S., Klein, C., Lindsey, S., Kear, M., 2008. Effects of dairy farming intensification on nitrous oxide emissions. Plant Soil. 309, 227–237. https://doi.org/10.1007/s11104-007-9444-9.

Luo, J., Saggar, S., van der Weerden, T., de Klein, C., 2019. Quantification of nitrous oxide emissions and emission factors from beef and dairy cattle excreta deposited on grazed pastoral hill lands. Agric. Ecosyst. Environ. 270, 103–113. https://doi.org/10.1016/j.agee.2018.10.020.

Maier, R., Hörtnagl, L., Buchmann, N., 2022. Greenhouse gas fluxes (CO2, N2O and CH4) of pea and maize during two cropping seasons: drivers, budgets, and emission factors

for nitrous oxide. Sci. Total. Environ. 849, 157541. https://doi.org/10.1016/j.scitotenv.2022.157541.
Maire, J., Krol, D., Pasquier, D., Cowan, N., Skiba, U., Rees, R.M., Reay, D., Lamigan, G. J., Richards, K.G., 2020. Nitrogen fertiliser interactions with urine deposit affect nitrous oxide emissions from grazed grasslands. Agric. Ecosyst. Environ. 290, 106784. https://doi.org/10.1016/j.agee.2019.106784.
Mauder M. and Foken T. (2004) Documentation and Instruction Manual of the Eddy Covariance Software Package TK3 (update). Arbeitsergebn, Univ Bayreuth, Abt Mikrometeorol, ISSN 1614-8916.
MeteoSwiss (2022) https://www.meteoswiss.admin.ch/climate/the-climate-of-switzerland/climate-normals/climate-diagrams-and-normals-per-station.html. Accessed 24 November 2022.
Moncrieff, J., Clement, R., Finnigan, J., Meyers, T., 2004. Averaging, detrending, and filtering of eddy covariance time series. *Handbook of Micrometeorology: A guide for Surface Flux Measurement and Analysis*. Springer Netherlands, Dordrecht, pp. 7–31.
Moncrieff, J., Malhi, Y., Leuning, R., 1996. The propagation of errors in long term measurements of land atmosphere fluxes of carbon and water. Global Change Biol 2, 231–240. https://doi.org/10.1111/j.1365-2486.1996.tb00075.x.
Murphy, R.M., Saunders, M., Richards, K.G., Krol, D.J., Gebremichael, A.W., Rambaud, J., Cowan, N., Lanigan, G.J., 2022. Nitrous oxide emission factors from an intensively grazed temperate grassland: a comparison of cumulative emissions determined by eddy covariance and static chamber methods. Agric. Ecosyst. Environ. 423, 107725. https://doi.org/10.1016/j.agee.2021.107725.
Neftel, A., Spirig, C., Ammann, C., 2008. Application and test of a simple tool for operational footprint evaluations. Environ. Pollut. 152, 644–652. https://doi.org/10.1016/j.envpol.2007.06.062.
Nemitz, E., Mammarella, I., Ibrom, A., Aurela, M., Burba, G., Dengel, S., Gielen, B., Grelle, A., Heinesch, B., Herbst, M., Hörtnagl, L., Klemedtsson, L., Lindroth, A., Lohila, A., McDermitt, K.D., Meier, P., Merbold, L., Nelson, D., Nicolini, G., Zahniser, M., 2018. Standardisation of eddy-covariance flux measurements of methane and nitrous oxide. Int. Agrophys. 32, 517–549. https://doi.org/10.1515/intag-2017-0042.
O'Connell, C.S., Anthony, T.L., Mayes, M.A., Pérez, T., Sihi, D., Silver, W.L., 2022. Utilizing novel field and data exploration methods to explore hot moments in high-frequency soil nitrous oxide emissions data: opportunities and challenges. Front. For. Glob. Change 5, 674348. https://doi.org/10.3389/ffgc.2022.674348.
Pedersen, A.R., Petersen, S.O., Schelde, K., 2010. A comprehensive approach to soil-atmosphere trace-gas flux estimation with static chambers. Eur. J. Soil. Sci. 61, 888–902. https://doi.org/10.1111/j.1365-2389.2010.01291.x.
Öquist, M.G., Nilsson, M., Sörensson, F., Kasimir-Klemedtsson, A., Persson, T., Weslien, P., Klemedtsson, L., 2004. Nitrous oxide production in a forest soil at low temperatures – processes and environmental controls. FEMS. Microbiol. Ecol. 49, 371–378. https://doi.org/10.1016/j.femsec.2004.04.006.
Reinsch, T., Malisch, C., Loges, R., Taube, F., 2020. Nitrous oxide emissions from grass–clover swards as influenced by sward age and biological nitrogen fixation. Grass. Forage Sci. 75, 372–384. https://doi.org/10.1111/gfs.12496.
Perlman, J., Hijmans, R.J., Horwath, W.R., 2014. A metamodeling approach to estimate global N_2O emissions from agricultural soils. Glob. Ecol. Biogeogr. 23, 912–924. https://doi.org/10.1111/geb.12166.
Rokach, L., Maimon, O., 2005. Decision trees. In: Maimon, O., Rokach, L. (Eds.), Data Mining and Knowledge Discovery Handbook. Springer, Boston, MA. https://doi.org/10.1007/0-387-25465-X_9.
Russelle, M.P., 1992. Nitrogen cycling in pasture and range. J. Prod. Agric. 5, 13–23. https://doi.org/10.2134/jpa1992.0013.
Savage, K., Phillips, R., Davidson, E., 2014. High temporal frequency measurements of greenhouse gas emissions from soils. Biogeosciences. 11, 2709–2720. https://doi.org/10.5194/bg-11-2709-2014.
Schils, R.L.M., van Groeningen, J.W., Velthof, G.L., Kuikman, P.J., 2008. Nitrous oxide emissions from multiple combined applications of fertiliser and cattle slurry to grassland. Plant Soil. 310, 89–101. https://doi.org/10.1007/s11104-008-9632-2.
Schmid, M., Neftel, A., Riedo, M., Fuhrer, J., 2001. Process-based modelling of nitrous oxide emissions from different nitrogen sources in mown grassland. Nutr. Cycl. Agroecosyst. 60, 177–187.
Selbie, D.R., 2015. The challenge of the urine patch for managing nitrogen in grazed pasture systems. Adv Agron 129, 229–292. https://doi.org/10.1016/bs.agron.2014.09.004.
Shi, A., Chakrawal, A., Manzoni, S., Fischer, B.M.C., Nunan, N., Herrmann, A.M., 2021. Substrate spatial heterogeneity reduces soil microbial activity. Soil Biol. Biochem. 152, 108068. https://doi.org/10.1016/j.soilbio.2020.108068.
Singh, P., Mehra, P., Fang, Y., Dougherty, W., Saggar, S., 2021. Nitrous oxide emissions from cow urine patches in an intensively managed grassland: influence of nitrogen loading under contrasting soil moisture. Sci. Total Environ 757, 143790. https://doi.org/10.1016/j.scitotenv.2020.143790.
Taki, R., Wagner-Riddle, C., Parkin, G., Gordon, R., VanderZaag, A., 2019. Comparison of two gap-filling techniques for nitrous oxide fluxes from agricultural soil. Can. J. Soil Sci. 99, 12–24. https://doi.org/10.1139/cjss-2018-0041.
Treweek, G., Di, H.J., Cameron, K.C., Podolyan, A., 2016. Simulated animal trampling of a free-draining stony soil stimulated denitrifier growth and increased nitrous oxide emissions. Soil. Use Manage 32, 455–464. https://doi.org/10.1111/sum.12281.
van der Weerden, T.J., Clough, T.J., Styles, T.M., 2013. Using near-continuous measurements of N2O emission from urine-affected soil to guide manual gas sampling regimes. New Zealand J. Agric. Res. 56, 60–76. https://doi.org/10.1080/00288233.2012.747548.
van Groeningen, J.W., Kasper, G.J., Velthof, G.L., van den Pol-van Dasselaar, A., Kuikman, P.J., 2004. Nitrous oxide emissions from silage maize fields under different mineral nitrogen fertilizer and slurry applications. Plant Soil. 263, 101–111.
van Groeningen, J.W., Kuikman, P.J., De Groot, W.J.M., Velthof, G.L., 2005a. Nitrous oxide emission from urine-treated soil as influenced by urine composition and soil physical conditions. Soil. Biol. Biochem. 37, 463–473. https://doi.org/10.1016/j.soilbio.2004.08.009.
van Groenigen, J.W., Velthof, G.L., Van der Bolt, F.J.E., Vos, A., Kuikman, P.J., 2005b. Seasonal variation in N_2O emissions from urine patches: effects of urine concentration, soil compaction and dung. Plant Soil. 273, 15–27.
Vinzent, B., et al., 2017. Efficacy of agronomic strategies for mitigation of after-harvest N_2O emissions of winter oilseed rape. Eur. J. Agronomy 89, 88–96. https://doi.org/10.1016/j.eja.2017.06.009.
Voglmeier, K., Jocher, M., Häni, C., Ammann, C., 2018. Ammonia emission measurements of an intensively grazed pasture. Biogeosciences. 15, 4593–4608. https://doi.org/10.5194/bg-15-4593-2018.
Voglmeier, K., Six, J., Jocher, M., Ammann, C., 2019. Grazing-related nitrous oxide emissions: from patch scale to field scale. Biogeosciences. 16, 1685–1703. https://doi.org/10.5194/bg-16-1685-2019.
Voglmeier, K., Six, J., Jocher, M., Ammann, C., 2020. Soil greenhouse gas budget of two intensively managed grazing systems. Agric. For. Meteorol. 287, 107960. https://doi.org/10.1016/j.agrformet.2020.107960.
Wagner-Riddle, C., Congreves, K.A., Abalos, D., Berg, A.A., Brown, S.E., Ambadan, J.T., Gao, X., Tenuta, M., 2017. Globally important nitrous oxide emissions from croplands induced by freeze–thaw cycles. Nat. Geosci. 10, 279–283.
Walling, E., Vaneeckhaute, C., 2020. Greenhouse gas emissions from inorganic and organic fertilizer production and use: a review of emission factors and their variability. J. Environ. Manage 276, 111211. https://doi.org/10.1016/j.jenvman.2020.111211.
Wang, W., Park, G., Reeves, S., Zahmel, M., Heenan, M., Salter, B., 2016. Nitrous oxide emission and fertiliser nitrogen efficiency in a tropical sugarcane cropping system applied with different formulations of urea. Soil. Res. 54, 572–584. https://doi.org/10.1071/SR15314.
Wang, K., Zheng, X.H., Pihlatie, M., Vesala, T., Liu, C.Y., Haapanala, S., Mammarella, I., Rannik, Ü., Liu, H.Z., 2013. Comparison between static chamber and tunable diode laser-based eddy covariance techniques for measuring nitrous oxide fluxes from a cotton field. Agric. For. Meteorol. 171, 9–19. https://doi.org/10.1016/j.agrformet.2012.11.009.
Wecking, A.R., Wall, A.M., Liáng, L.L., Lindsey, S.B., Luo, J., Campbell, D.I., Schipper, L. A., 2020. Reconciling annual nitrous oxide emissions of an intensively grazed dairy pasture determined by eddy covariance and emission factors. Agric. Ecosyst. Environ. 287, 106646. https://doi.org/10.1016/j.agee.2019.106646.
Xie, Y., Zhang, M., Xiao, W., Zhao, J., Huang, W., Zhang, Z., Hu, Y., Qin, Z., Jia, L., Pu, Y., Chu, H., Wang, J., Liu, S., Lee, X., 2022. Nitrous oxide flux observed with tall-tower eddy covariance over a heterogeneous rice cultivation landscape. Sci. Total. Environ. 810, 152210. https://doi.org/10.1016/j.scitotenv.2021.152210.
Zheng, Y., Pei, J.-Y., Fang, C., Peñuelas, J., Sardans, J., Xiong, Y.-C., Li, D-F, Ke, W.-B., Ye, J.-S., 2023. Determining the harvest frequency to maintain grassland productivity and minimum nutrient removal from soil. Plant Soil. 487, 79–91. https://doi.org/10.1007/s11104-023-05907-w, 2023.